



Active Lithium Injection for a Real Time Control of the Divertor Heat Flux for Fusion Devices

M. Ono¹ · R. Raman²

Accepted: 16 September 2023 / Published online: 12 October 2023

© The Author(s), under exclusive licence to Springer Science+Business Media, LLC, part of Springer Nature 2023

Abstract

When the local heat flux exceeds specified flux limit, tungsten PFC surfaces can be damaged, which is not acceptable for a reliable reactor operations. The divertor PFCs are typically designed for a specific heat flux limit usually assuming an average steady-state heat flux which is typically 5–10 MW/m². However, in addition to steady-state heat flux, fusion reactor divertor PFCs could experience transient heat fluxes such as ELMs and/or other magnetic reconnection events which can deposit large transient heat fluxes onto the divertor PFCs. The transient divertor heat flux could be significantly larger than the steady-state heat flux which could damage the solid PFC surfaces. The divertor heat flux can be subjected to additional complications such as the uncertainties in the the divertor strike point heat flux projection. Moreover, there are additional experimental observations of non-axisymmetric power flux which can occur under non-axisymmetric magnetic perturbations. The liquid lithium (LL) PFCs is more resilient against such transient heat fluxes as they could evaporate LL as needed and the lost LL can be then replenished afterward. In this paper, we analyze a case for a transient divertor heat pulse of 1 MJ in 10 ms for a ITER-size reactor. This is a small perturbation ($\sim 0.1\%$) to the expected plasma stored energy compared to the previously analyzed case of 20 MJ heat pulse. Even with this relatively modest heat pulse, the LL surface undergoes ~ 100 °C temperature rise. However, the resulting LL surface heating without rapid cooldown mechanism could lead to excessive LL evaporation continuing well after the transient heat flux resulting in a significant Li injection of ~ 0.6 mol in about a 200 ms period. This amount of Li injection could cause plasma dilution and performance degradation. On the other hand, an active Li injection capability if optimized could prevent the LL surface temperature rise and thus reducing subsequent Li evaporation into the plasma by a factor of 7 compared to the passive LL PFC case. A crucial tool of active Li injection is a rapid response pellet injector which could inject light impurity pellets before the excessive heat flux could reach the divertor plate causing serious damage. A simple pellet ablation model suggests a favorable pellet deposition profile for smaller ~ 0.1 mm radius pellet with ~ 10 – 20 m/s velocity. Moreover, if it is possible to inject from the private flux region, the pellet injection efficiency into the high heat flux strike point region can be as high as 80% compared to $\sim 50\%$ for the injection from outer radius region. The pellet deposition efficiency can be further improved by designing a shell-pellet which can burst when a certain ablation fraction is reached. A possible implementation technique using an inductive pellet injector with a rapid time response of a few msec is proposed here which can be tested in NSTX-U.

Keywords Transient heat flux · Divertor · Liquid lithium · Active lithium injection

Introduction

While tungsten has been regarded as the most suitable solid divertor material [1–3], many challenges including possible surface melting and cracking have been pointed out. Such

This work was supported by DoE Contract No. DE-AC02-09CH11466 and DE-SC0006757. One of authors (M.O.) thanks Drs. S. Kaye, R. Lunsford, W. Choe, Y. Hirooka and N. Tamura for valuable suggestions.

✉ M. Ono
mono@pppl.gov

¹ Princeton Plasma Physics Laboratory,
PO Box 451, Princeton, NJ 08543, USA

² University of Washington, Seattle, USA

deleterious modification of the PFC surfaces must be prevented to develop reliable plasma facing components (PFCs) [4]. Most divertor PFCs are designed based on the maximum steady-state operational heat flux limits of $\sim 5\text{--}10\text{ MW/m}^2$ so the reactor must operate below this maximum heat handling capability of PFCs. Furthermore, for induced radiation safety, the use of reduced activation ferritic steel will be required for the divertor heat sink in a fusion power reactor, which would worsen the heat removal situation. To maximize the heat conduction or heat removal capability, the thickness of the material between the divertor PFCs and the coolant is usually minimized typically to $\sim 10\text{ mm}$. A thinner tungsten design would improve the heat removal capability but that would increase the possibility of a coolant leak into the reactor chamber which must be avoided. This thin material design feature also limits the amount of material erosion such PFCs can tolerate [5–7].

In addition to the steady-state heat loads for fusion reactor systems, there are serious concerns over potential damages to the PFCs by the transient heat fluxes accompanying ELMs and/or other uncontrolled magnetic events. The transient high heat flux can easily cause reattachment of detached divertor operations which can further exacerbate the heat flux situation. While the transient events are best to be avoided in future reactors, it is prudent to plan in case such an event occurs. In tokamaks and spherical tokamaks, H-mode is known to trigger ELMs with a significant heat pulse burst [8]. One should also point out that even for steady-state heat flux, the divertor strike point width predictions are quite varied so the reliable divertor strike point heat flux prediction maybe difficult for future devices. Moreover, with some non-axisymmetric fields, the divertor heat flux could have correspondingly non-axisymmetric features whereby the local heat flux peak could significantly exceed the toroidally symmetric heat flux values.

The liquid lithium (LL) PFCs is also more resilient against such localized transient heat fluxes. As the heat flux impinging on LL, the rising LL surface temperature increases the LL evaporation which would reduce the local heat flux through Li radiative cooling. The lost LL can be then replenished afterward as shown in Fig. 1. We call the passive LL divertor protection mechanism RLLD (radiative LL divertor) [9]. With relatively modest transient heat flux of 1 MJ, we show that much more Li than necessary is evaporated during the slow cool-down phase. To minimize the total amount of Li evaporation, we show that active Li injection capability (ARLLD) can reduce the total Li injection amount by a factor of 6–7 [10].

A schematic depiction of RLLD and ARLLD is shown in Fig. 1. Such a tool if successfully developed could not only prevent divertor PFC damages against transient events

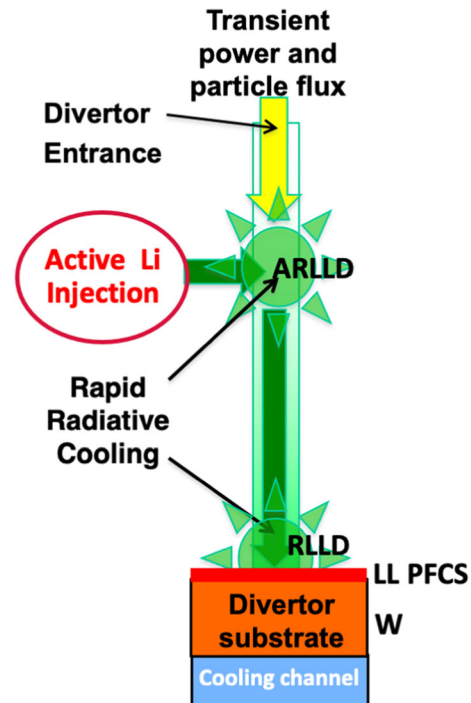


Fig. 1 A schematic of active and passive Li divertor injection for transient heat flux control

but also could eventually be used to effectively control the divertor heat flux level onto the PFC surfaces and allow them to stay within the design specification, ensuring the long-term viability of the fusion reactor divertor system.

In the previous publication on this topic, we showed the active Li injection could in principle prevent a large transient heat flux [10]. The present work extends the previous work to evaluate a case for more modest transient heat pulse of $\sim 1\text{ MJ}$ compared to the previous $\sim 20\text{ MJ}$. The ITER device with the major radius of 6.2 m is expected to have 200 MJ of plasma thermal energy so $\sim 1\text{ MJ}$ energy expulsion represents only 0.5% of the plasma stored energy [2]. We shall use the ITER device parameter as a prototype of a fusion reactor in this present work. While the device size is expected to remain ITER-like, the future reactor is expected to increase fusion performance by a factor of $\sim 4\text{--}6$ with plasma stored energy approaching 1 GJ. In such a plasma, 1 MJ energy expulsion is only 0.1% of the stored energy. One might note for ELM-based transient heat flux, smaller ELMs tend to occur at higher frequency compared to larger ones [8].

We also investigated candidate pellet size and speed required for an optimum active Li injection for divertor flux control. In “[Divertor Transient Heat Pulse Model](#)” section, the transient heat pulse 1-D model is briefly discussed. In “[Passive LL Divertor Behavior Under Transient Heat Flux](#)” section, a time dependent diffusive model is introduced to describe the transient heat flux onto the

passive LL divertor (LLD). In “Active Control of LL Divertor Under Transient Heat Flux” section, a feasibility of controlling the transient heat flux by an active Li injection is discussed. In “Developing Active Li Pellet Injection” section, we describe a Li pellet injection set up. In “Outboard and Inboard Li Pellet Injections” section, outboard and inboard Li pellet injections are discussed. In “Conclusions and Discussion” Section, conclusions and discussion are given.

Divertor Transient Heat Pulse Model

The time dependent 1D diffusion model to analyze the transient heat flux is shown in Fig. 2 [11]. The tungsten material is assumed here to be 10 mm which is typically specified to mitigate against erosion of the W armour for fusion reactor divertor PFCs. The cooling channel of 200 °C is located below tungsten substrate. The following time dependent 1-D diffusion equation was solved for the tungsten substrate subdivided into 40 sections with the temperature boundary condition at the cooling channel fixed at the coolant temperature of 200 °C:

$$\frac{\partial T}{\partial t} = \alpha \frac{\partial^2 T}{\partial z^2} \quad (1)$$

where z is the spatial variation perpendicular from the surface to the cooling channel, $\alpha = \frac{\kappa}{\rho c_p}$ is the thermal diffusivity coefficient, κ is thermal conductivity (W/(m-K)), c_p is the specific heat capacity (J/(kg-K)), and ρ is density (kg/m³). A time step of 10 ms is used to avoid numerical instability. The temperature dependent tungsten properties are given in Ref. [12].

The surface temperature rise is determined by the heat flux impinging on the surface and the time dependent

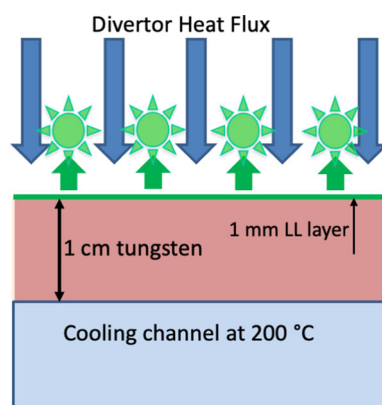


Fig. 2 1-D model of divertor PFCs. The base substrate is tungsten with 1 cm thickness with a cooling channel temperature which is fixed at 200 °C. LL layer of 1 mm thickness is added over the tungsten substrate to simulate RLLD

diffusion equation is evolved with the time step of 10 ms. The blackbody surface radiation cooling is included in the calculation though it played a negligible role for the present problem. The LL surface layer is assumed to be 1 mm thick. This thin LL layer was chosen to facilitate the heat transfer to the tungsten substrate and help the LL adhere to the substrate material through surface tensions.

The transient heat flux imposes additional challenges on divertor PFCs since the relevant transient time scale of ~ 10 ms is much shorter than the characteristic time of heat conduction from the PFC surface to the cooling channel which is ~ 1 s. For the solid divertor, we assume that the divertor heat flux is impinging on the tungsten surface. To simulate the LL divertor (LLD), we assume 1 mm LL layer as shown in Fig. 2. The transient heat flux is simulated assuming 1 MJ heat pulse with 10 ms square pulse duration. The divertor heat flux is estimated assuming the device major radius to be ITER-like ~ 500 cm and the axisymmetric heat flux radial width of 10 cm, making the total strike point area of ~ 3.8 m². The situation can be more severe if the heat flux is not uniform.

In Fig. 3, we plot the surface temperature T_s evolution for the 10 ms transient pulse as labelled for a pure tungsten surface without any Li layer (as shown in Fig. 2 without 1 mm LL layer). The base steady-state heat load of 10 MW/m² is assumed here making the tungsten surface temperature to be ~ 1000 °C in this model. As shown in Fig. 3, while the temperature rises to ~ 1400 °C can be rapid, the cool down time is relatively slow compared to the transit time scale. The fact that the temperature is still rising linearly at the end of the heat pulse show that the cooling channel is not playing a role which is consistent with the slower conduction cooling time scale. Here we assumed the cooling channel is at 200 °C. If the cooling channel is at 300 °C which is preferred in some reactor

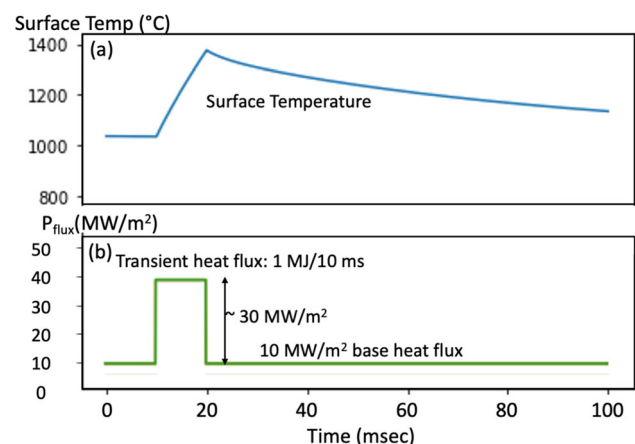


Fig. 3 (a) 1-D model of tungsten PFC surface temperature evolution (b) for a transient heat pulse of 10 ms duration with 1 MJ energy and the base heat load of 10 MW/m²

divertor studies [5], the corresponding temperature rise is 100 °C larger reaching 1500 °C. Some studies find that tungsten recrystallization starts to occur above 1300 °C, therefore, it is desired to limit the tungsten temperature rise to below 1300 °C.

Passive LL Divertor Behavior Under Transient Heat Flux

In this section, we examine the effect of the 1 MJ transient heat pulse as shown in Fig. 3 for a LL divertor configuration modeled in Fig. 2. For steady-state operations, the RLLD could provide a simple solution for handling high heat flux. As the heat flux is increased at the divertor strike point, the temperature rises at the LLD surface which increases the LL evaporation rate.

In Fig. 4, the Li evaporation rate is shown for a typical reactor size LL divertor strike point with $R = 5$ m and the strike point radial width of $DR = 10$ cm. As can be seen, the Li evaporation rate goes up rapidly for temperatures above 500 °C. Once the temperature increases above 700 °C, the evaporation into plasma becomes significant. It is about 10 mol/sec which can cause plasma dilution and performance degradation. One should note that 10 mol/sec Li injection rate represents replacing the entire divertor plasma with Li even for a short particle confinement time of 1 ms. So, it is prudent to not let the LL divertor PFC strike point surface temperature to exceed 700 °C. The evaporated Li would enter the plasma, and the ionization and radiative process described in the following section could reduce the heat flux until a balance of proper amount of Li evaporation and heat flux is reached.

The non-coronal equilibrium radiative heat dissipation has the potential of radiating a large amount of heat, well over two orders of magnitude larger than the evaporative

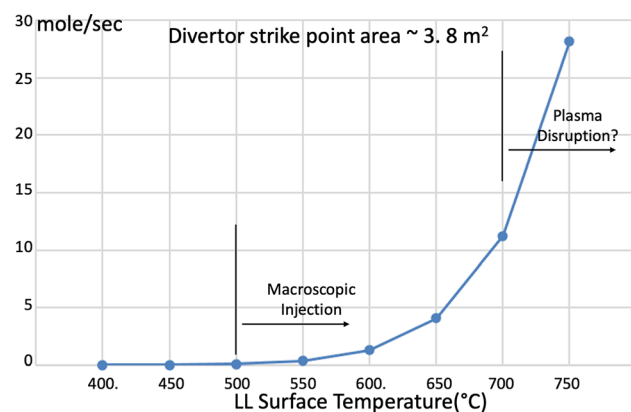


Fig. 4 Li evaporation rate (mole/sec) vs. the divertor temperature. The divertor strike point area is ~ 3.8 m² with $R_0 = 5$ m and $Dx = 10$ cm

process [13, 14]. Indeed, high Li radiation level of \sim few hundred eV per Li atom was reported in an experiment in the tokamak T11M [14]. This non-coronal radiation is larger by 2–3 orders of magnitude compared to the coronal equilibrium value [13, 15, 16]. Based on the most recent non-coronal calculations by Mavrin [17], one can expect sufficient radiated energy level of ~ 20 –50 MJ/mole for typical reactor divertor plasma parameters where the particle confinement time is relatively short ~ 1 –10 ms. This is because the injected Li atom is highly radiative only during the initial period of its injection into the plasma as it undergoes rapid ionization and radiative processes.

In Fig. 5, using the non-coronal radiation values calculated in Ref. 17, we show the total radiated energy per mole of injection into a divertor plasma in a reactor-like regime. It should be noted that while the radiated power is largest at the beginning of the injection, the integrated radiated energy still increases with the plasma confinement time as the injected Li still radiates at some albeit lower level. For a reactor size divertor plasma, the particle confinement time could be ≥ 1 ms and T_e up to 300 eV as indicated in Fig. 5. In this regime, the radiated energy level of up to 50 MJ/mole can be expected which is larger compared to the RLLD region in Fig. 5. Also the difference between 1 and 10 ms confinement time is relatively small for the high temperature regime which reduces the uncertainty of the effectiveness of the active Li injection. For the passive Li injection (RLLD), the Li is assumed to be evaporated by divertor plasma impinging on its LL coated divertor PFC surfaces. Through plasma interaction, the evaporated Li enters the divertor plasma along the field lines. So, for RLLD, one would expect colder, ≤ 30 eV, temperature plasma as the main interaction region is near the divertor plate as indicated in Fig. 5. Since the interaction is near the PFC, the confinement time is probably closer to 1 ms. This lower temperature regime may still provide effective

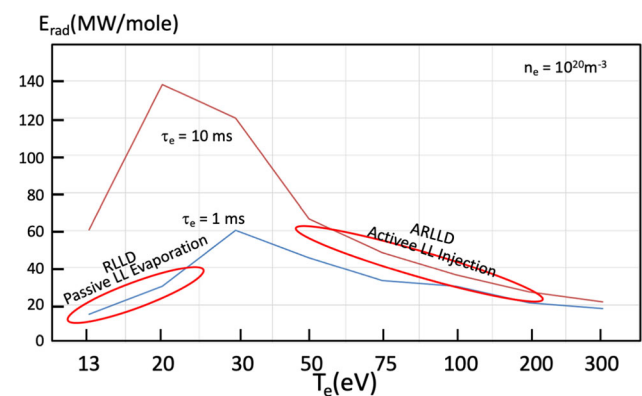


Fig. 5 Radiated energy per mole of injected Li into divertor plasma with $n_e = 10^{20}$ m⁻³ for particle confinement time as labelled as a function of electron temperature. Possible reactor operating regime for ARLLD and RLLD are as indicated

radiative cooling because of the active radiation band near 20–50 eV range. The radiation tends to remain quite strong above ~ 13 eV as shown in Fig. 5 which is well satisfied in much of the divertor high heat flux region. This is consistent with the previous 1D model calculations in the references [9, 10]. One important side benefit of impurity injection in addition to its rapid radiation cooling is injection of additional cold electrons associated with ionizing impurity ions which increases the local electron density and reduces electron temperature proportionally.

As shown in Fig. 6, the passive RLLD is simulated with the model shown in Fig. 2. As shown in Fig. 6a, the LL surface temperature is near 600 °C for steady-state RLLD operation handling about 10 MW/m² steady-state heat flux. At 600 °C, the resulting lithium evaporation provides a steady-state solution. As the heat flux is increased due to the transient heat pulse at the divertor strike point, the resulting temperature rise (a) at the LLD surface increases the LL evaporation (b) as shown in Fig. 6b. The evaporated Li would enter the plasma, and the ionization and radiative processes described previously could reduce the heat flux until a balance of proper amount of Li evaporation and heat flux is achieved. This property of RLLD makes Li evaporation quite effective in reducing the divertor heat flux to a desired level and also provides natural protection for the divertor substrate. When the heat flux reaching the LL surface is reduced (c), the Li surface temperature rise saturates near 700 °C as shown in Fig. 6a, resulting in less than 100 °C temperature rise compared to a much larger value of over 300 °C for the pure tungsten case. This shows that the LL surface does indeed protect the tungsten substrate from the high transient heat flux. One potential issue

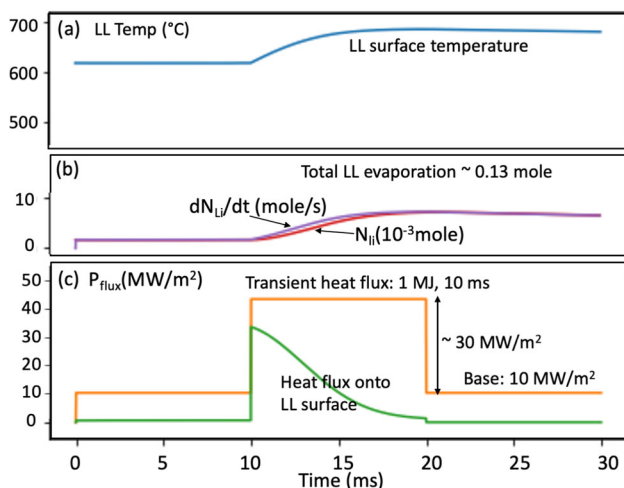


Fig. 6 RLLD divertor during the transient heat pulse of 1 MJ in 10 ms. **a** LL surface temperature evolution. **b** Evaporated Li injection rate dN_{Li}/dt and total Li population N_{Li} , and **c** transient heat flux into divertor 1 MJ in 10 ms over the steady-state 10 MW/m² heat flux and onto Li surface as labelled

of the RLLD is that while the surface temperature rises rapidly to ~ 700 °C, the surface temperature only cools down slowly as shown in Fig. 6a since there is no rapid cooling mechanism available. The blackbody radiation is weak and the conduction cooling is slow ~ 1 s. In the figure, the Li injection rate dN_{Li}/dt , Li particle inventory N_{Li} and heat fluxes are illustrated to show the time evolution behavior.

In Fig. 7, we show the longer time behavior of the case shown in Fig. 6 to assess the cooling behavior. As shown in Fig. 7a, the LL surface temperature drops only slowly after the transient heat pulse and the Li evaporation continues in the meantime. The integrated total Li injection is 0.69 mol which is more than five times the Li injection of 0.13 mol during the transient time as shown in Fig. 6. The injection of 0.69 mol of Li in 0.2 s corresponds to more than 3 mol/sec of Li injection rate which is quite large. This excessive Li injection could cause degradation of plasma performance if not more serious plasma disruption. This issue motivates the active radiative divertor concept as discussed in “Active Control of LL Divertor Under Transient Heat Flux” section. By actively injecting light impurities, it is possible to prevent the LL surface temperature rise thus minimize the amount of Li injection.

Active Control of LL Divertor Under Transient Heat Flux

For the ARLLD regime, the active injection should take place in more upstream divertor region (as depicted in Fig. 1) which has larger confinement time of up to 10 ms and higher divertor temperature of ~ 100 –200 eV as indicated in Fig. 5. As can be seen in the figure, ARLLD

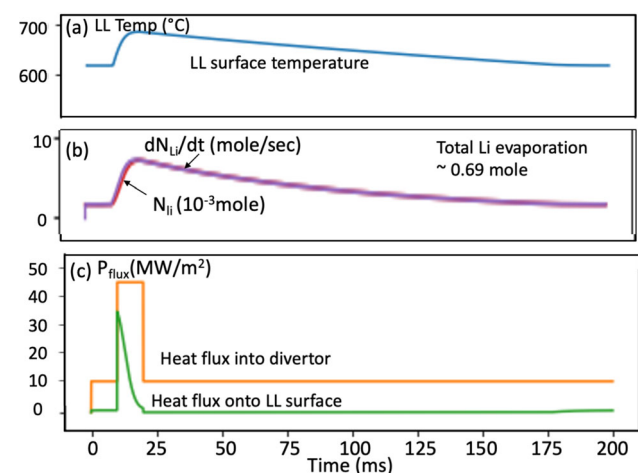


Fig. 7 Longer terms evolution of RLLD divertor during the transient heat pulse of 1 MJ in 10 ms as in the case shown in Fig. 6 with 10 MW/m² steady-state heat flux

regime shows $\sim 30\text{--}50$ MJ/mole of radiated energy. This means that a small fraction of a mole injected into the divertor plasma would be sufficient to radiatively cool the 1 MJ of heat pulse before reaching the divertor.

In Fig. 8, an optimized ARLLD case is shown which can essentially prevent the LL surface temperature rise. For this to be possible, it would be necessary to start the Li injection about 4 ms before the arrival of the transient heat pulse as shown in Fig. 8. This pre-pulse injection gives the time for the injected Li to disperse in the divertor plasma before the transient heat pulse arrives. The injected Li is larger than the ones needed to counter the steady-state heat flux level of 10 MW/m^2 so the heat flux quickly goes to zero until the time of the heat pulse arrival. This early Li injection helps the Li particle inventory in the plasma above the divertor plate to increase sufficiently. The increased radiation from the divertor plasma prevents much of the transient heat pulse flux from reaching the LL divertor surface resulting. As a result, the LL surface temperature remains about the same and it does not see the larger temperature rise seen in Fig. 6 for the RLLD case. Overall, the LL surface temperature remains relatively unchanged for this ARLLD case.

While pre-heat-pulse injection might not be easy, if one can develop a sufficient understanding of the precursor behavior of the transient events such as for ELMs and other MHD events, one may have a sufficient time to inject Li prior to the arrival of the transient heat pulse into the divertor region as shown in Fig. 8. Alternatively, if the ELM frequency is nearly constant, Li could also be injected at the same frequency. If an EM fails to occur, the primary consequence maybe a reduction in heat flux in the divertor plate for that cycle. Once the heat pulse is over,

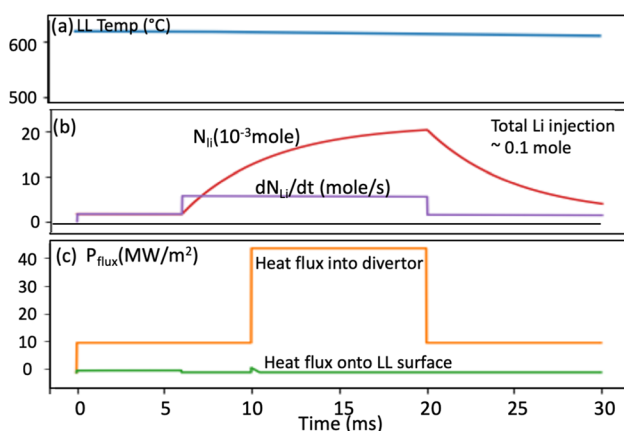


Fig. 8 An optimized ARLLD divertor during the transient heat pulse of 1 MJ in 10 ms. **a** LL surface temperature evolution. **b** Evaporated Li injection rate dN_{Li}/dt and total Li population N_{Li} , and **c** transient heat flux into divertor 1 MJ in 10 ms over the steady-state 10 MW m^2 heat flux and onto Li surface as labelled

the Li density decays with the Li particle confinement time of ~ 5 ms assumed here as shown in Fig. 8.

The total injected Li for this optimized ARLLD case is only 0.1 mol compared to 0.69 mol for the passive LLD case shown in Fig. 6. This active injection therefore can reduce the amount of Li injection by a factor of 7 compared the passive case. This small Li injection during the transient event should minimize the Li fuel dilution and plasma degradation problem. We should also note that the low-Z impurities such as Li should not cause an impurity accumulation problem compared to high-Z impurities such as tungsten from the neo-classical transport point of view. It is needless to say that the smaller the LLD temperature rise, the less the resulting Li influx into the plasma. So, even if the active Li injection is not perfect, it still has a beneficial effect of reducing the amount of Li injection as long as it can reduce the LLD temperature rise. We shall now discuss the implementation of the active Li injection system.

Developing Active Li Pellet Injection

For effective transient heat flux mitigation, it is crucial to deposit the Li at the flux surfaces where the majority of the heat flux is flowing. This would naturally be those flux surfaces just outside of the last closed flux surface or the X-point. Since the heat flux is flowing along the spiral path into the divertor, the heat flux geometry is necessarily 3D.

In Fig. 9a, the ITER-like divertor flux surfaces are shown. In order to illustrate the field line pitch, in Fig. 9b, the toroidal field excursion parameter $R(x) + \cos(F)$ is plotted as a function of vertical position along the field line for each flux surface where $R(x)$ is the flux major radius location at the x-point vertical position and F is the toroidal angle radian along the field line. So, one radial oscillation represents one toroidal transit. Naturally, near the X-point, due to the shallow pitch angle, radial oscillation increases. With shallow pitch angle, the injection region can intersect the heat flux more effectively. With vertical coverage of one oscillation length, one could ensure the full heat flux interception. Therefore, near the x-point, the required vertical coverage is ~ 10 cm as marked by the red circles. Since it is likely that the injection will need to take place at more than one toroidal location, the required coverage then becomes ~ 5 cm for each of the two locations, etc. To make the cooling relatively toroidally balanced, it would be desirable to inject at a few $\sim 3\text{--}4$ toroidal locations. Multiple injection points would also ensure injection reliability against potential misfiring.

The inductive pellet injector (IPI) described in Ref. [11] is well suited for the simultaneous injection. In a larger size reactor system, it might be also be possible to inject from the private flux region as depicted by “inboard” injection

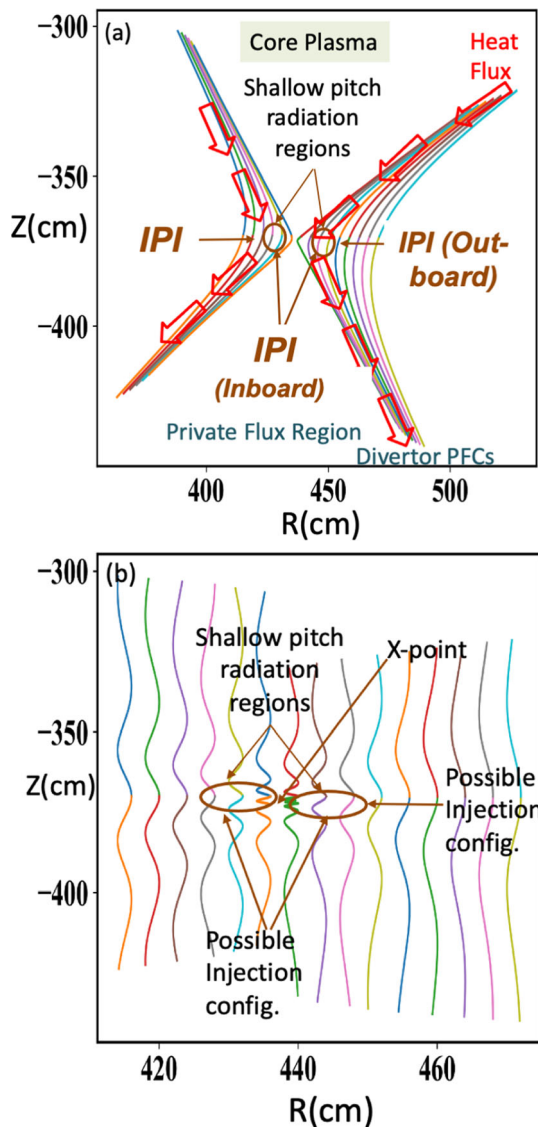


Fig. 9 Possible active Li injection configuration in ITER-like divertor configuration. **a** Divertor flux surfaces near the divertor x-point. **b** Toroidal excursion $R(x) + \cos(F)$ vs and vertical excursion along the ray starting at the x-point vertical location

in Fig. 9 as it could readily access both high field and low field sides of the x-point region. For an ST-based reactor, the heat flux is likely to be predominantly in the low-field-side of the x-point but for a tokamak-based reactor, the heat flux is more balanced such that it maybe necessary to mitigate both sides of the x-point. Since the high heat flux region is near the x-point, private region injection will enable very short access paths to the high heat flux regions, this therefore enables faster response as the pellet only has to travel a short distance. Another important consideration is the size and speed of the pellet as described in “[Outboard and Inboard Li Pellet Injections](#)” section.

Outboard and Inboard Li Pellet Injections

Since the divertor plasma by definition is outside of the last closed flux surface, the pellet penetration is not an issue. A reliable rapid response time is more important than the injection velocity for example. For this reason, we proposed the electromagnetically driven Inductive Pellet Injector (IPI) system [11, 18]. The IPI system has an advantage of its flexibility to injection any type of pellets with no inherent limit to the number of pellets to be injected.

Here we use a simple pellet ablation model to simulate the pellet penetration and deposition. For low Z pellets such as Li the following semi-analytic formula based of neutral gas shielding (NGS) model was used [19, 20]:

$$G \sim \left[\frac{T_e}{2000} \right]^{5/3} \left[\frac{r_p}{0.2} \right]^{4/3} \left[\frac{n_e}{10^{14}} \right]^{1/3} \tag{2}$$

where G (g/s) is the ablation rate, T_e (eV) is the electron temperature, n_e (1/cc) is the density, and r_p (cm) is the pellet radius.

In terms of the divertor plasma parameters, we assumed the profiles shown in Fig. 10 where (a) the strike point region is flat with a maximum temperature 200 eV and (b) the density is $1 \times 10^{20}/m^3$ (b) with radial width of 10 cm. The density and temperature decay with 20 cm e-folding length for the radially outward direction from the strike point. For the radially inward direction, we assume a 5 cm gap between the strike point and the inner wall which depicts the private region. The density and temperature are

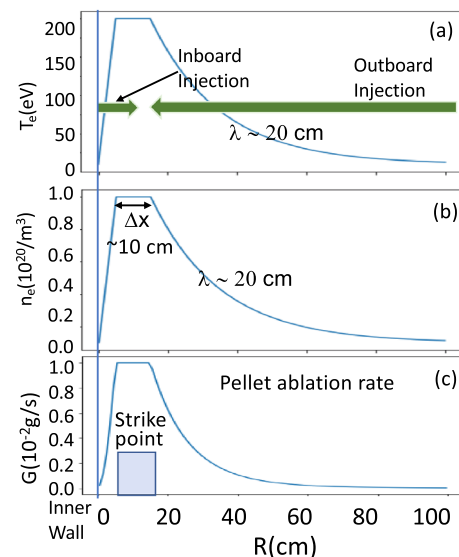


Fig. 10 Pellet injection set up for inboard and outboard injections. **a** Radial electron temperature profile. **b** Radial density profile. **c** The corresponding pellet ablation rate of $r = 0.2$ mm pellet

assumed to drop off linearly between the strike point and the inner (private flux) wall.

For the outboard injection, the injector is assumed to be located at $R = 100$ cm. For the inboard injection, the injector is assumed to be located at $R = 0$ cm. For this model, clearly the inboard injection has an advantage in terms of the distance from the injector to the strike point plasma. It is of course possible to locate the outboard injector closer to the strike point.

In Fig. 10c, the corresponding pellet erosion or ablation rate of the pellet with 0.2 mm radius is shown. As shown in the figure, the pellet ablation rate strongly peaks at the strike point due to the maximum temperature and density as it depends strongly on the temperature as shown in Eq. (2). This strongly peaked behavior makes the Li deposition inside the divertor strike point feasible. Using the pellet injection model, we investigated a number of scenarios for both inboard and outboard injected pellets.

Outboard Pellet Injection

In Fig. 11, we show the outboard injection of a relatively small pellet of size 0.1 mm radius for various pellet speeds. The pellet weight fraction plot shows how much deposition occurs at a certain location. As can be seen from the figure, a higher speed pellet penetrates deeper into the divertor plasma as expected. In fact, for pellets with speed of less than 10 m/s, much of the pellet deposition takes place before reaching the strike point region so it would not be effective in quenching the high divertor heat flux. The maximum pellet fraction deposition of 50% occurs when the pellet speed reaches 20 m/s.

In Fig. 12, we show the case of a larger pellet size of 0.4 mm radius. For the larger pellet size of 4 times radius, about a factor of 10 reduction in the injection velocity is

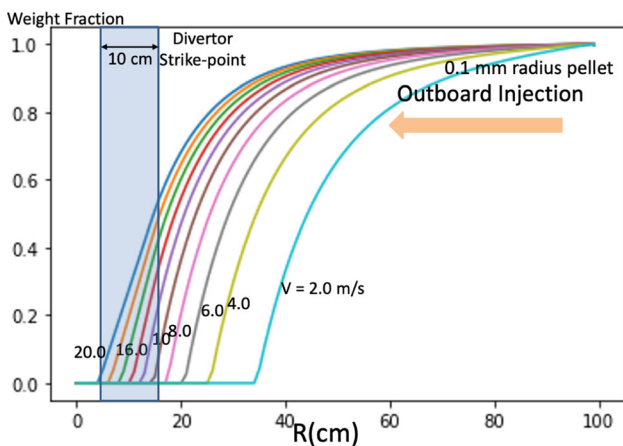


Fig. 11. 0.1 mm radius pellet injection set up for outboard injections. The pellet weight fraction as a function of radial position is plotted for various pellet velocities as labeled

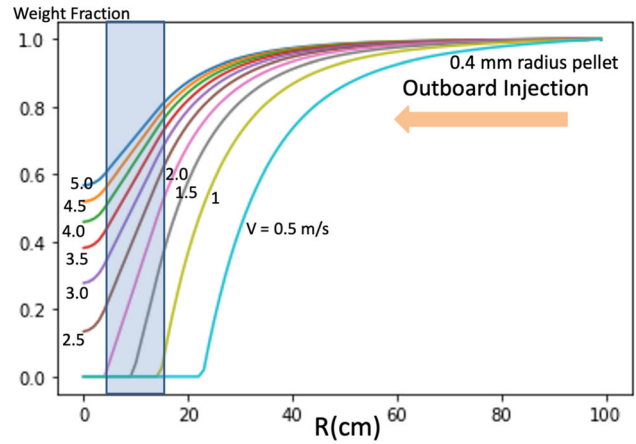


Fig. 12. 0.4 mm radius pellet injection set up for outboard injections. The pellet weight fraction as a function of radial position is plotted for various pellet velocities as labeled

required for a similar penetration. The 2 m/s velocity appears to be optimum for deposition at the strike point region which corresponds to about 50% deposition similar to the 0.1 mm case. In fact, the optimized deposition remains about 50% for the pellet size of 0.2 mm and 0.3 mm radii as well. Therefore this 50% efficiency appears to be a typical limit for the outboard injection.

Inboard Pellet Injection

In Fig. 13, we show the inboard injection of relatively small pellet of size of 0.1 mm radius for various pellet speeds. While the velocity range is similar to the outboard case, the deposition efficiency can be quite high $\sim 80\%$. Unlike the outboard injection cases, the lower velocity range ≤ 10 m/sec actually gives higher deposition fraction for the inboard injection. The higher velocity causes overshoot of pellets. So the injection velocity must be

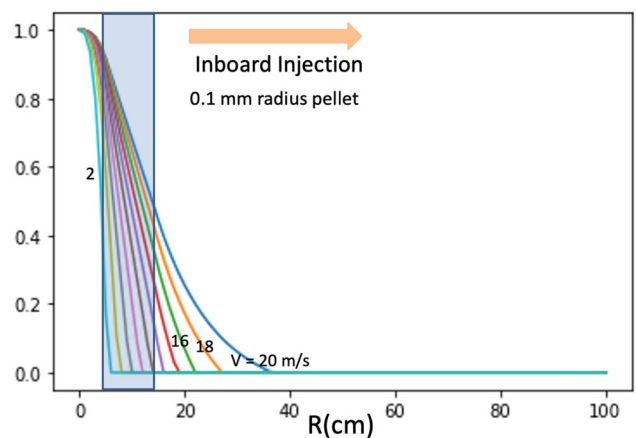


Fig. 13. 0.1 mm radius pellet injection set up for inboard injections. The pellet weight fraction as a function of radial position is plotted for various pellet velocities as labeled

lower for the inboard injection particularly for the larger pellets.

In Fig. 14, the inboard injection of larger size pellet of 0.4 mm radius as shown as a function of various velocities. The desired pellet velocity which gives high $\sim 80\%$ deposition efficiency is ≤ 1 m/sec which is a factor of 10 lower compared to the 0.1 mm radius case. Overall, the optimized efficiency for the inboard injection appears to be $\sim 80\%$ compared to $\sim 50\%$ for the outboard injector. Also, the travel distance for the inboard injection is relatively short so the delay time can be made correspondingly shorter. It might be advantageous to inject 0.1 mm size pellet at ≤ 10 m/s which combines both high strike point ablation fraction with relatively short delay time.

The IPI can indeed inject a “cup” full of small pellets ~ 0.1 mm at a specified velocity of 10 m/s which might be well suited for the inboard injection. The injection deposition efficiency maybe further improved by using a special pellet type such as a shell pellet which can burst at a certain location and deliver the content for more controlled local Li deposition as demonstrated in the TESPEL experiments [21]. The shell burst location could be controlled with the shell thickness.

Conclusions and Discussion

The extreme heat flux anticipated in fusion reactor divertor PFCs is perhaps the most challenging technology issue for fusion energy development. Most divertor PFCs are designed based on the maximum steady-state heat flux operational limits. However, in addition to the steady-state heat flux, the fusion reactor divertor PFCs could also experience significant transient heat flux such as from ELMs and/or magnetic reconnection events which can

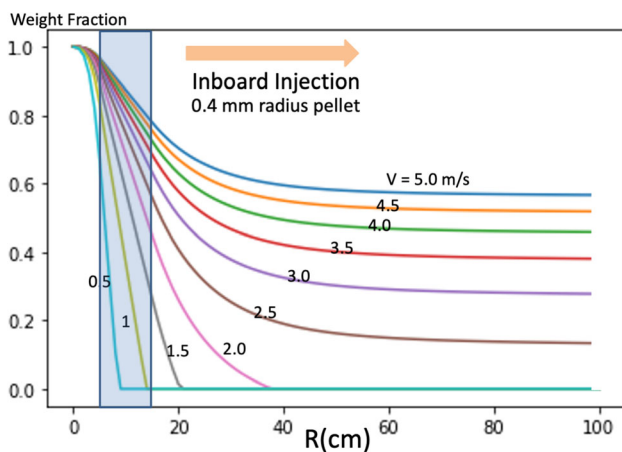


Fig. 14. 0.4 mm radius pellet injection set up for inboard injections. The pellet weight fraction as a function of radial position is plotted for various pellet velocities as labeled

deposit large transient heat flux onto the divertor PFCs. One might expect that a significant fraction of plasma stored energy can be expelled in a short time.

In this paper, we investigated a transient heat pulse of ~ 1 MJ on divertor PFCs which is a modest value and much more likely to occur compared to the 10–20 MJ transient heat pulse case previously investigated. Here we showed that even 1 MJ of energy (less than 0.1% of plasma stored energy) if expelled in a short time scale of ~ 10 ms, would result in a factor of 4 increase in the divertor heat flux over the based steady-state heat load of ~ 10 MW/m². For pure tungsten PFCs, the divertor strike-point surface could experience significant tungsten surface temperature rise of 300 °C, raising the surface temperature to 1400 °C. While this would not melt or destroy the tungsten surfaces, it is still a significant temperature rise which needed to be carefully monitored.

For a LL covered divertor PFCs, the LL surface experiences temperature rise which enhances the LL evaporation and injection of LL into the divertor plasma. The LL surface temperature rises from ~ 600 to 700 °C which in this temperature range, significantly increases the LL evaporation rate. For the transient case of 10 ms pulse width, we find the steady-state active cooling through conduction plays essentially no role as the cooling process is quite slow ~ 1 s. The blackbody radiation cooling is also relatively small. For the passive RLLD case, while the divertor temperature rise is limited due to the evaporating Li, and the divertor surface is protected, the subsequent slow cooling of LL surfaces causes excessive LL evaporation which could degrade the plasma performance.

The active injection of LL (ARLLD) looks promising since it can prevent the undesirable temperature rise of the LL PFC surfaces and thus prevent excessive LL evaporation. Indeed, the active Li injection, if optimized, could reduce the Li injection amount by a factor of 7. For actual active injection implementation, we propose an inductively driven injector which can deliver the pellet at a very fast time response of ~ 1 ms with high reliability [10].

In terms of the injection geometry, it is suggested that the optimum injection region could be near the X-point where the poloidal field pitch becomes small facilitating good toroidal coverage. This suggests that a few injectors (3–4) distributed toroidally might be sufficient to attain a full toroidal coverage. The utilization of multiple injectors could also minimize the effect of possible misfiring of one of the injectors.

In terms the actual pellet injection, inboard and outboard configurations are investigated. The outboard pellet injection assumed the placement of the injector at ~ 1 m radially outward position away from the strike point. The smaller pellet with $R \sim 0.1$ mm with relatively high velocity of ~ 20 m/sec can deposit Li inside the high heat

flux strike-point region. An injection from the private region which we term inboard injection has an advantage of relative proximity ~ 5 cm to the strike-point region. For this injection, small pellets of $R = 0.1$ mm with velocity of 10 m/sec would be 80% effective for the strike-point Li deposition. The inboard injection is also advantageous in terms of having a faster response time.

The present ARLLD concept should apply well to a pure tungsten divertor to prevent an excessive tungsten temperature rise which could cause recrystallization and surface cracking. In this case, another low Z material such as beryllium which has a similar radiative characteristic as lithium could also be used [22].

One can test the ARLLD concept on NSTX-U using an ILLI. The experiment should provide necessary data such as the amount of radiation cooling that can be achieved per given Li injection and the optimum injection location and pellet velocity that does not lead to plasma performance degradation. Once the active injection Li radiative cooling is well understood, it could become a versatile actuator to control the divertor PFC surface temperature to within a specified limit against any type of non-local and/or transient heat flux.

Author Contributions MO wrote the main manuscript, prepared all figures, and ran computer simulations presented in the manuscript. RR performed calculations related to the inductive pellet injector system and reviewed the manuscript.

Funding We acknowledge support of this work by the U.S. Department of Energy, Office of Science/Fusion Energy Sciences under DoE Contract No. DE-AC02-09CH11466 and DE-SC0006757.

Availability of Data and Materials The data that support the findings of this study are available from the corresponding author upon reasonable request.

Declarations

Conflict of interest We declare that the authors have no competing interests as defined by Springer, or other interests that might be perceived to influence the results and/or discussion reported in this paper.

Ethical Approval Not applicable.

References

1. Magnetic Fusion Energy Science Research Needs Workshop report, June 2009, <http://burningplasma.org/web/ReNeW/ReNeW.report.web2.pdf>
2. R. Aymar et al., *Plasma Phys. Control. Fusion* **44**, 519 (2002)
3. R.A. Pitts et al., *Nucl. Mater. Energy* **20**, 100696 (2019)
4. R.E. Nygren et al., *J. Nucl. Mater.* **417**, 451 (2011)
5. R. Tobita et al., *Nucl. Fusion* **49**, 075029 (2009)
6. E. Visca et al., *Fusion Eng. Des.* **87**, 941 (2012)
7. X.R. Wang et al., *2012 Fusion Eng. Des.* **87**, 732 (2012)
8. A.W. Leonard, *Phys. Plasmas* **21**, 090501 (2014)
9. M. Ono et al., *Nucl. Fusion* **53**, 113030 (2013)
10. M. Ono et al., *Fusion Eng. Des.* **89**, 2838 (2014)
11. M. Ono, R. Raman, *J. Fusion Energy* **39**, 402–410 (2020)
12. Documentation Series No 29, IAEA, Vienna 1991. “Blanket, Shield Design and Material Data Base”.
13. T.D. Rognlien, M.E. Rensink, *Phys. Plasmas* **9**, 2120 (2002)
14. S.V. Mirnov et al., *J. Nucl. Matter* **S224-S228** 438 (2013)
15. V.B. Lazarev et al., *1999 26th EPS Conf. on Controlled Fusion and Plasma Physics (Maastricht, The Netherlands, 14–18 June 1999)* (ECA) vol 231 p 845
16. V.A. Evtikhin et al., *Plasma Phys. Control. Fusion* **44**, 955 (2002)
17. A.A. Mavrin, *J Fusion Energy* **36**, 161 (2017)
18. R. Raman et al., *IEEE Trans. Plasma Sci.* **44**(9), 1547 (2016)
19. P.B. Park et al., *Nucl. Fusion* **17**, 539 (1977)
20. R. Samulyak et al., *Nucl. Fusion* **47**, 103 (2007)
21. N. Tamura et al., *IOP Conf. Ser. J. Phys. Conf. Ser.* **823**, 012003 (2017)
22. M. Ono, R. Raman, et al., *IAEA-CN-286-1003* (2021)

Publisher's Note Springer Nature remains neutral with regard to jurisdictional claims in published maps and institutional affiliations.

Springer Nature or its licensor (e.g. a society or other partner) holds exclusive rights to this article under a publishing agreement with the author(s) or other rightsholder(s); author self-archiving of the accepted manuscript version of this article is solely governed by the terms of such publishing agreement and applicable law.